

Particle production from gluon-nucleon interactions in relativistic heavy ion collisions

Yong-Ping Fu,¹ Fei-Jie Huang,² and Qi-Hui Chen³

¹Department of Physics, West Yunnan University, Lincang 677000, China

² Department of Physics, Kunming University, Kunming 650214, China

³ School of Physical Science and Technology, Southwest Jiaotong University, Chengdu 610031, China

(Dated: May 2, 2024)

We propose a particle production mechanism analogous to the particle photoproduction processes, arising from the gluon-nucleon interactions in relativistic heavy ion collisions. The comparison is made on the effect of the gluon-nucleon interactions on the photon production in Au+Au collisions at $\sqrt{s_{NN}}=200$ GeV and Pb+Pb collisions at $\sqrt{s_{NN}}=2.76$ TeV. The numerical results indicate that as the collision energy increases, the contribution of gluon-nucleon interactions becomes more prominent.

I. INTRODUCTION

Relativistic heavy ion collisions represent a prominent research focus in high energy physics. The high energy heavy ion collision experiments provide insights into various aspects of particle interactions, including the perturbative Quantum Chromodynamics (pQCD) that governs nucleon-nucleon deep inelastic scattering and their underlying parton structures. Moreover, the relativistic heavy ion collisions provide a unique opportunity to investigate the properties of hot and dense matter composed of quarks and gluons, known as quark-gluon plasma (QGP).

In relativistic heavy ion collisions, the jets produced from the parton collisions lose energy due to gluon radiation in the hot medium, this phenomenon is called jet quenching [1–3]. Jets in a hot medium can radiate gluons similarly to the bremsstrahlung of electrons. In the color deconfined QGP, jet quarks with color charge radiate soft gluons due to multiple scattering with the hot particles [4–7]. The suppression of hadron spectra from relativistic heavy ion collisions observed by detectors at Relativistic Heavy Ion Collider (RHIC) and Large Hadron Collider (LHC) can provide evidences for the existence of this effect [8–10]. Without the influence of the thermal medium, partons within nucleons can also radiate gluons through hard scattering [11–14]. However, the gluon radiation discussed above occurs in the final states of particle scattering. Due to color confinement, it is not possible for initial state partons within nucleons to directly radiate gluons in hadronic collisions.

In this paper, we consider the situation in which some nucleons of heavy ions have already collided and thermalized in the initial stage of the relativistic heavy ion collisions. The collective behavior of hadronic particles has been observed in high multiplicity pp , pA and dA collision experiments at RHIC and LHC [15–23]. During the initial stage of the relativistic heavy ion collisions, some small hot systems may have already appeared. The remaining nucleons (or partons within the nucleons) in the heavy ion, which have not yet collided, will collide and interact with these small hot systems. If the mean free path of the incident parton is large compared to the

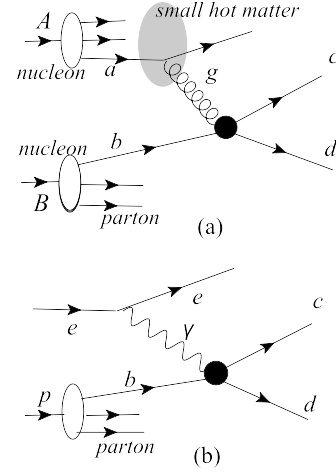


FIG. 1: (a) Illustration of gluon-nucleon interactions, the gluon radiates from the initial state parton a due to scattering with the small hot medium. (b) The e - p deep inelastic scattering induced by the photon-nucleon interactions.

Debye screened length, an initial state quark a of the nucleon A collides into the small hot medium, and scatters with a thermal parton, the initial state quark a will radiate a high energy gluon. The radiated gluon will then interact with a parton b of another incident nucleon B , the process [Fig.1(a)] is similar to the particle photoproduction processes in electron-proton deep inelastic scattering at HERA [24] [Fig.1(b)]. Through the above analysis, we can observe that under the condition of color deconfinement, the high energy gluons radiated by initial state quarks are entirely capable of undergoing hard scattering with other cold partons. However, in cold nuclear matter, gluons emitted by initial state partons rapidly fragment into jets due to the color confinement effect.

The paper is organized as follows: In Sec. II, we discuss the scattering amplitude for the quark scattering that leads to the gluon radiation. The gluon spectrum inside an initial state quark is calculated. In Sec. III, we derive the differential cross section for particles production resulting from the gluon-nucleon interactions in relativistic heavy ion collisions. In Sec. IV, we employ

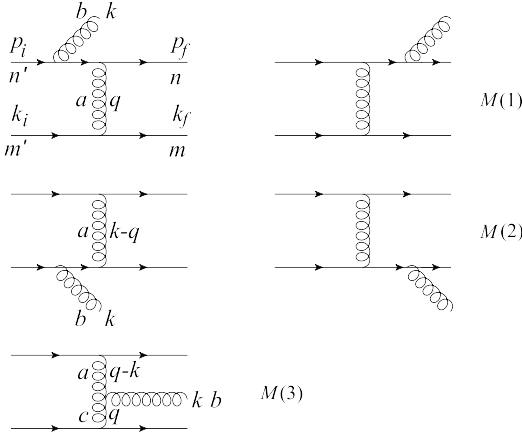


FIG. 2: Feynman diagrams for gluon radiation in leading order (LO) quark scattering.

photon probes to analyze the contribution of the gluon-nucleon interactions at RHIC and LHC energies. Finally, a summary is provided in Sec. V.

II. GLUON RADIATION OF THE INITIAL STATE QUARK

We first review the amplitude of quark scattering that leads to gluon radiation [7, 11], the Feynman diagrams satisfying gauge invariance are shown in Fig.2. The complete LO amplitude of gluon radiation induced by the quark scattering is given by

$$\begin{aligned}
M = & \frac{igM_{el}}{T_{BB'}^a T_{AA'}^a} \left\{ \left[\frac{\varepsilon \cdot p_f}{k \cdot p_f} (T^b T^a)_{nn'} - \frac{\varepsilon \cdot p_i}{k \cdot p_i} (T^a T^b)_{nn'} \right] T_{mm'}^a \right. \\
& + \frac{q^2}{(k-q)^2} \left[\frac{\varepsilon \cdot k_f}{k \cdot k_f} (T^b T^a)_{mm'} - \frac{\varepsilon \cdot k_i}{k \cdot k_i} (T^a T^b)_{mm'} \right] T_{nn'}^a \\
& \left. + \frac{2\varepsilon \cdot q}{(k-q)^2} [T^b, T^a]_{nn'} T_{mm'}^a \right\}, \quad (1)
\end{aligned}$$

where T^a is the SU(3) generator with the color indices n, n', m, m', A, A', B and B' of quarks. Here a and b are the non-Abelian gauge field indices. The three terms of the above equation represent the scattering amplitudes $M(1)$, $M(2)$ and $M(3)$ in the Feynman diagrams as shown in Fig.2, respectively. The radiated gluon momentum k satisfies the on-shell condition $k^2=0$, and the polarization ε satisfies $\varepsilon \cdot k=0$. The Born scattering amplitude is

$$M_{el} = \frac{g^2}{q^2} T_{nn'}^a T_{mm'}^a \bar{u}(p_f) \gamma_\mu u(p_i) \bar{u}(k_f) \gamma^\mu u(k_i), \quad (2)$$

The light-cone initial momenta p_i of the beam parton in the nucleon and k_i of the target parton in the small hot medium are defined as

$$p_i = (p^+, 0, \mathbf{0}_\perp), \quad (3)$$

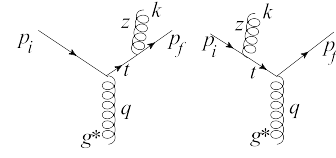


FIG. 3: The amplitudes for the LO gluon radiation.

$$k_i = (m_q, m_q, \mathbf{0}_\perp), \quad (4)$$

where the effective temperature-dependent mass is $m_q(T) = \sqrt{2\pi\alpha_s^T/3T}$ [25], here the temperature-dependent coupling constant is $\alpha_s^T = 6\pi/[(33 - 2N_F) \ln(8T/T_c)]$ with critical temperature $T_c=160$ MeV, and the flavor number of the quarks $N_f \approx 2.5$ to account the mass of s quark [26]. The final momenta of the beam and target partons are

$$p_f = p_i + q - k, \quad (5)$$

$$k_f = k_i - q. \quad (6)$$

The GW and BDMPS models have considered the effect of soft gluon radiation, and found that the amplitude $M(2)$ in Fig.2 is negligible compared to $M(1)$ and $M(3)$ in the light-cone gauge [4-7]. Here we show that in the high energy gluon radiation condition, $k \gg q$, the amplitude $M(2)$ and $M(3)$ are depressed by the terms of $q^2/(q-k)^2$ and $\varepsilon \cdot q/(q-k)^2$, respectively. Only the projectile diagrams $M(1)$ contribute significantly to the radiation of high energy gluon. In the leading pole approximation the differential cross section of the gluon radiation (Fig.3) can be expressed as

$$\frac{d\sigma}{\sigma_0 dz dt} = \frac{\alpha_s}{2\pi t} P_{gq}(z), \quad (7)$$

where the Mandelstam variable $t = (p_i + q)^2 = (k + p_f)^2$, the splitting function $P_{gq} = C_F [1 + (1-z)^2]/z$ with $C_F = 3/4$. z is the momentum fraction of the radiated gluon. By integrating over the Lorentz invariant t , we obtain the gluon radiation spectrum of an initial state quark:

$$f_{gq} = \int dt \frac{d\sigma}{\sigma_0 dz dt} = \frac{\alpha_s}{2\pi} P_{gq}(z) \ln \frac{t_{max}}{t_{min}}, \quad (8)$$

the values of t_{max} and t_{min} will discuss in Section III.

III. PARTICLES PRODUCTION INDUCED BY GLUON-NUCLEON INTERACTIONS

The invariant differential cross section for particle production from the gluon-nucleon interactions in Fig.1(a) can be derived as following

$$\begin{aligned}
\frac{d\sigma_{g-n}}{d^2p_T dy} = & \sum_{a,b} \frac{1}{\pi} \int_{x_a^{min}}^1 dx_a \int_{x_b^{min}}^1 dx_b G_a^A(x_a, Q^2) f_{ga}(z_a, T) \\
& \times G_b^B(x_b, Q^2) \frac{x_a x_b z_a}{x_a x_b - x_a x_2} \frac{d\hat{\sigma}_{gb \rightarrow cd}}{d\hat{t}}(\hat{s}, \hat{u}, \hat{t}), \quad (9)
\end{aligned}$$

where $x_{a,b}$ and z_a are the momentum fractions of the initial state parton and radiated gluon, respectively. Q is the momentum scale. The momentum fractions with the transverse momentum p_T and rapidity y are given by

$$x_a^{min} = \frac{p_T e^y}{\sqrt{s_{NN}} - p_T e^{-y}}, \quad (10)$$

$$x_b^{min} = \frac{x_a p_T e^{-y}}{x_a \sqrt{s_{NN}} - p_T e^y}, \quad (11)$$

$$z_a = \frac{x_b p_T e^y}{x_a x_b \sqrt{s_{NN}} - x_a p_T e^{-y}}, \quad (12)$$

here $\sqrt{s_{NN}}$ is the center-of-mass energy of the colliding nucleons. The parton distribution for the nucleus is given by

$$G_i^A(x_i, Q^2) = R_i^A(x_i, Q^2) [Z F_i^p(x_i, Q^2) + (A - Z) F_i^n(x_i, Q^2)] / A, \quad (13)$$

where $R_i^A(x_i, Q^2)$ is the nuclear modification factor, Z is the proton number, A is the nucleon number. The functions $F_i^p(x_i, Q^2)$ and $F_i^n(x_i, Q^2)$ are the parton distribution function (PDF) of the proton and neutron, respectively.

The Mandelstam variables \hat{s} , \hat{u} and \hat{t} of the differential cross sections $d\hat{\sigma}/d\hat{t}(gb \rightarrow cd)$ are

$$\hat{s} = x_a x_b z_a s_{NN}, \quad (14)$$

$$\hat{u} = -x_b p_T e^y \sqrt{s_{NN}}, \quad (15)$$

$$\hat{t} = -x_a z_a p_T e^{-y} \sqrt{s_{NN}}. \quad (16)$$

In the high energy gluon radiation limit, $k^+ \approx p^+$, the radiated gluon is in the forward direction. In this case, we obtain the results $p_{imax} \approx (\sqrt{\hat{s}}, 0, \mathbf{0}_\perp)$ and $q_{max} \approx (m_q, m_q, \mathbf{0}_\perp)$, then logarithmic scale t_{max} in Eq.(8) is

$$t_{max} = \sqrt{\hat{s}} m_q(T) + m_q(T)^2. \quad (17)$$

Taking into account the scale parameter of pQCD, we choose $t_{min} = (0.2 \text{ GeV})^2$ [27]. The parameter t_{max} indicates that the gluon radiation spectrum depends on the temperature of the QGP droplets formed in the early stage of relativistic heavy ion collisions.

IV. APPLICATION IN PHOTON PRODUCTION

Through the analysis of particle production processes, we observed that, in comparison to the invariant differential cross section of direct particles production, the contribution of the gluon-nucleon scattering processes is suppressed by the QCD running coupling constant α_s in the

gluon radiation spectral function f_{gq} . As an application of gluon-nucleon scattering, we will now discuss particles that can be detected by the detectors, such as photons. The electromagnetic radiation produced from relativistic heavy ion collisions is a useful probe for investigating pQCD and the QGP. Photons do not directly participate in strong interactions, and the mean free path of photons is larger than that of the collision system. Consequently, photons can escape to the detector almost undistorted through the strongly interacting system.

During the initial parton collisions stage, the direct photons are primarily produced by the quark-antiquark annihilation ($q\bar{q} \rightarrow g\gamma$) and the Compton scattering ($qg \rightarrow q\gamma$) [27]. The invariant cross section from the two processes is expressed as

$$\frac{d\sigma_{dir\gamma}}{d^2p_T dy} = \sum_{a,b} \frac{1}{\pi} \int_{x_a^{min}}^1 dx_a G_a^A(x_a, Q^2) G_b^B(x_b, Q^2) \times \frac{x_a x_b}{x_a - x_1} \frac{d\hat{\sigma}_{ab \rightarrow \gamma d}}{d\hat{t}}(\hat{s}, \hat{u}, \hat{t}), \quad (18)$$

here the momentum fraction x_b is

$$x_b = \frac{x_a p_T e^{-y}}{x_a \sqrt{s_{NN}} - p_T e^y}, \quad (19)$$

and the value of x_a^{min} is consistent with Eq.(10). The Mandelstam variables of the the subprocesses $d\hat{\sigma}/d\hat{t}(ab \rightarrow \gamma d)$ are

$$\hat{s} = x_a x_b s_{NN}, \quad (20)$$

$$\hat{u} = -x_b p_T e^y \sqrt{s_{NN}}, \quad (21)$$

$$\hat{t} = -x_a p_T e^{-y} \sqrt{s_{NN}}. \quad (22)$$

In addition to direct photon production, fragmentation photons are also the primary source of large transverse-momentum photons in initial parton collisions [27]. The invariant cross section for the $AB \rightarrow (c \rightarrow \gamma)X$ interaction can be written as

$$\frac{d\sigma_{fra\gamma}}{d^2p_T dy} = \sum_{a,b} \frac{1}{\pi} \int_{x_a^{min}}^1 dx_a \int_{x_b^{min}}^1 dx_b G_a^A(x_a, Q^2) G_b^B(x_b, Q^2) \times D_{\gamma c}(z_c, Q^2) \frac{1}{z_c} \frac{d\hat{\sigma}_{ab \rightarrow cd}}{d\hat{t}}(\hat{s}, \hat{u}, \hat{t}), \quad (23)$$

where the momentum fraction of the final state parton c is

$$z_c = \frac{p_T}{\sqrt{s_{NN}}} \left(\frac{e^y}{x_a} + \frac{e^{-y}}{x_b} \right). \quad (24)$$

The values of x_a^{min} and x_b^{min} are consistent with Eq.(10) and Eq.(11), respectively. The Mandelstam variables of the differential cross sections $d\hat{\sigma}/d\hat{t}(ab \rightarrow cd)$ are

$$\hat{s} = x_a x_b s_{NN}, \quad (25)$$

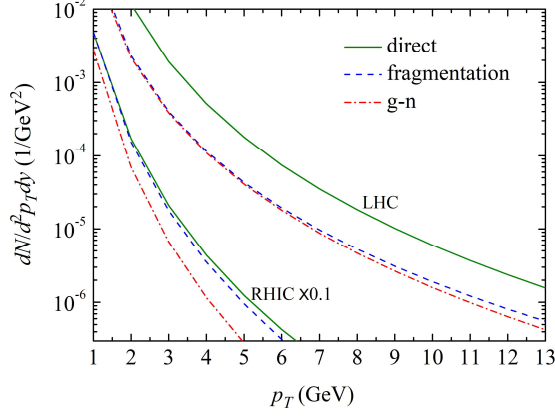


FIG. 4: Photon yields of the direct photons (solid line), fragmentation photons (dash line) and photons produced from the gluon-nucleon interactions (dash dot line) at RHIC and LHC energies.

$$\hat{u} = -\frac{x_b}{z_c} p_T e^y \sqrt{s_{NN}}, \quad (26)$$

$$\hat{t} = -\frac{x_a}{z_c} p_T e^{-y} \sqrt{s_{NN}}. \quad (27)$$

The effect of thermal medium induced jet energy loss on photon fragmentation $D_{\gamma c}^0$ is presented by the WHS phenomenological model [1–3], this approach is useful for studies of the parton energy loss of fragmentation function and multiple final state scattering. The probability for a jet to scatter n times within a distance $L (= n\lambda_q)$ in the thermal medium is provided as $P_n = (L/\lambda_q)^n e^{-L/\lambda_q} / n!$, where λ_q is the mean free path of the quark. The fragmentation function can be modified in the following form

$$D_{\gamma c}(z_c, Q^2) = C_n \sum_{n=0}^N P_n \frac{z_c^n}{z_c} D_{\gamma c}^0(z_c^n, Q^2) \quad (28)$$

where $C_n = 1 / (\sum_{n=0}^N P_n)$, $N = E_T^{\text{jet}} / \varepsilon$ is the scattering number, $E_T^{\text{jet}} = p_T / z_c$ is the transverse energy of the jet, and $z_c^n = z_c / (1 - \Delta E / E_T^{\text{jet}})$. The total energy loss ΔE of the quark and average energy loss per scattering ε are defined as follows:

$$\Delta E = \int_0^L \frac{dE}{dx} dx, \quad (29)$$

$$\varepsilon = \lambda_q \frac{dE}{dx}. \quad (30)$$

The energy loss dE/dx of jets crossing the hot and dense plasma is determined by the BDMPs model [4]

$$\frac{dE}{dx} = \frac{\alpha_s c_a \mu^2}{8\lambda_g} L \ln \frac{L}{\lambda_g}, \quad (31)$$

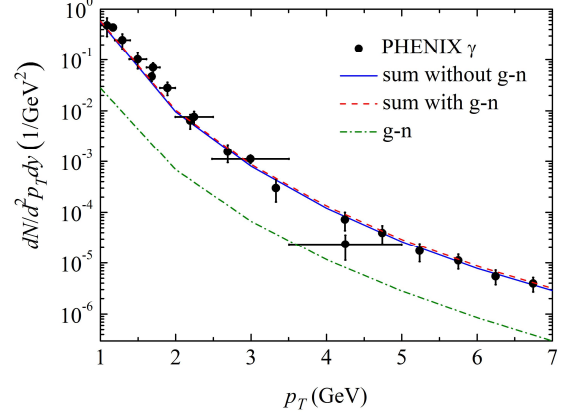


FIG. 5: Photon yields from the Au+Au collisions at $\sqrt{s_{NN}}=200$ GeV for 0-20% centrality class. The dashed line includes the sum of direct photons, fragmentation photons, jet-photon conversion, thermal photons from the QGP and HG phases, and photons produced from the gluon-nucleon interactions. The solid line does not include the contribution of the gluon-nucleon interactions. The dash dot line is the photon yield from the gluon-nucleon interactions. The data on photons are from the PHENIX experiments [28, 29].

where $c_a=4/3$ for quarks and 3 for gluon, the square of the Debye mass is $\mu^2 = 4\pi\alpha_s T^2$, $\lambda_g = \pi\mu^2 / [126\alpha_s^2 \zeta(3)T^3]$ and $\lambda_q = 9\lambda_g/4$ are the gluon and quark mean free path, respectively [7].

In the discussion of photon production, the leading-order subprocess of gluon-nucleon collision is the Compton scattering $gq \rightarrow \gamma q$ in Eq.(9). Although the invariant cross section magnitude for gluon-nucleon collisions [$O(\alpha_s^2\alpha)$] is smaller than the magnitude for direct photon production [$O(\alpha_s\alpha)$], we note that the invariant cross section for fragmentation photons [Eq.(23)] is of the same order as gluon-nucleon collisions [Eq.(9)]. In Fig.4, we present the yields of direct photons, fragmentation photons, and photons originating from the gluon-nucleon interactions in 0-20% Au+Au collisions at $\sqrt{s_{NN}}=200$ GeV and 0-20% Pb+Pb collisions at $\sqrt{s_{NN}}=2.76$ TeV. The photon yield is obtained by the following [30]

$$\frac{dN}{d^2p_T dy} = \frac{\langle N_{coll} \rangle}{\sigma_{inel}^{NN}} \frac{d\sigma}{d^2p_T dy}, \quad (32)$$

where $\langle N_{coll} \rangle$ is the average number of binary nucleon-nucleon collisions, σ_{inel}^{NN} is the inelastic nucleon-nucleon cross section. We use $\langle N_{coll} \rangle = 1210.8$ and 770.6 , $\sigma_{inel}^{NN} = 64$ and 40 mb, corresponding to the nucleon-nucleon collisions at $\sqrt{s_{NN}}=200$ GeV and 2.76 TeV, respectively [30–33]. In the numerical calculations, we use the CTEQ6L1 PDF [34] and EPS09 nuclear modifications [35], with a momentum scale chosen as $Q^2 = 4p_T^2$. We investigate photon production in the midrapidity region of Au+Au and Pb+Pb collisions.

In Au+Au collisions at RHIC, the contribution of gluon-nucleon interactions is not as pronounced as in

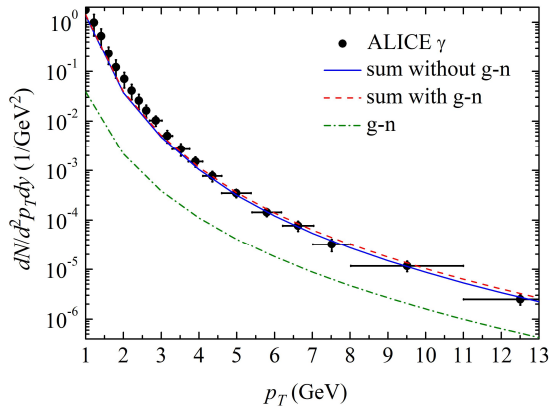


FIG. 6: Same as Fig.5 but for the Pb+Pb collisions at $\sqrt{s_{NN}}=2.76$ TeV for 0-20% centrality class. The data on photons are from the ALICE experiments [31].

Pb+Pb collisions at the LHC (Fig.4). We find that with increasing collision energy of nucleons, the contribution of gluon-nucleon interactions becomes increasingly prominent. In Pb+Pb collisions at $\sqrt{s_{NN}}=2.76$ TeV, the photon production from gluon-nucleon interactions is essentially comparable to the production of fragmentation photons. The direct photons remain the primary source. We use the parameterized photon fragmentation function by Owens [27]. The correction factors $K_{dir} \sim 1.5$ for RHIC and LHC, $K_{frag} \sim 1.8$ at RHIC and 1.4 at LHC are used to account for the next-to-leading order (NLO) corrections [30]. Since the subprocess of gluon-nucleon interactions is the Compton process $gq \rightarrow \gamma q$, the NLO correction factor is also chosen as $K_{n-g} \sim 1.5$ for RHIC and LHC.

Large transverse momentum photons are mainly produced by the interactions of the initial partons discussed above. Photons emitted from the QGP [25, 26, 36–43] and Hadronic Gas (HG) [41, 44–46] phases are mainly concentrated in the low transverse momentum region. Jets from cold component interactions colliding with the hot medium can also produce large transverse momentum photons [30, 47–50]. In Figs.5 and 6, we present the total photon yield from relativistic heavy ion collisions at RHIC and LHC energies. In addition to the photons produced from the gluon-nucleon interactions, contributions from prompt photons, thermal photons, and the jet-photon conversion are also included. The energy loss from the photon fragmentation in jets and the jet-photon conversion are both considered. For the calculation of the jet-photon conversion, the NLO correction factor for jet productions is chosen as $K_{jet} \sim 1.7$ for RHIC and 1.6 for LHC [30].

We mainly focus on the production of large transverse

momentum photons. Since thermal photons are primarily concentrated in the low transverse momentum region and the photons produced from interactions of the cold components are not prominent in this region, we adopt the 1+1D hydrodynamics for simplicity to calculate the evolution of hot matter [38, 51]. The initial conditions are chosen as $T_0=548$ and 658 MeV, $\tau_0=0.12$ and 0.1 fm/c for RHIC and LHC, respectively. Because the temperature of the small hot matter cannot be directly determined, we assume the temperature in the gluon radiation spectrum to be $T \sim 300$ MeV [21]. We also compare our results with the 1+2D hydrodynamic results by Gale et al. [43] to ensure that technical aspects are under control.

From the numerical results, it can be analyzed that in the Au+Au collisions at $\sqrt{s_{NN}}=200$ GeV, the contribution of the gluon-nucleon interactions on the total photon yield is $\sim 10\%$ in the region of $4 \text{ GeV} < p_T < 7 \text{ GeV}$ (Fig.5). However, as the energy increases to the LHC energy, the contribution of the gluon-nucleon interactions on the total photon yield becomes significant as shown in Fig.6. Starting from $p_T = 4$ GeV, the contribution of the gluon-nucleon interactions to the total photon yield becomes increasingly prominent, rising from a contribution rate of 10% at $p_T=4$ GeV to 19% at $p_T=13$ GeV.

V. SUMMARY

In this work we present calculations of the temperature dependent spectrum of high energy gluon radiation and the invariant differential cross section for particle production from the gluon-nucleon interactions in relativistic heavy ion collisions. Through calculations of photon production at RHIC and LHC energies, we demonstrate that in the large transverse momentum region, gluon-nucleon interactions make a noticeable contribution to particle production. This contribution of gluon-nucleon interactions is directly related to the nucleon-nucleon collision energy, and it becomes more pronounced with increasing collision energy, particularly in the LHC energies. In relativistic heavy ion collisions, the gluon-nucleon interactions can be one of the candidate mechanisms for particle production.

Acknowledgements

This work was supported by the Program for Innovative Research Team at Kunming University, the Program for Frontier Research Team at Kunming University 2023. Y. P. Fu acknowledges the support from the National Natural Science Foundation of China (Grant No.11805029).

-
- [1] X. N. Wang, Z. Huang, and I. Sarcevic, *Phys. Rev. Lett.* 77, 231 (1996).
- [2] X. N. Wang and Z. Huang, *Phys. Rev. C* 55, 3047 (1997).
- [3] X. N. Wang, *Phys. Rev. C* 58, 2321 (1998).
- [4] R. Baier, Y. L. Dokshitzer, A.H. Mueller, S. Peigne, and D. Schiff, *Nucl. Phys. B* 483, 291 (1997).
- [5] R. Baier, Y. L. Dokshitzer, A.H. Mueller, S. Peigne, and D. Schiff, *Nucl. Phys. B* 484, 265 (1997).
- [6] M. Gyulassy and X. N. Wang, *Nucl. Phys. B* 420, 583 (1994).
- [7] X. N. Wang, M. Gyulassy, and M. Plümer, *Phys. Rev. D* 51, 3436 (1995).
- [8] A. M. Sirunyan *et al.* (CMS Collaboration), *Phys. Rev. Lett.* 119, 082301 (2017).
- [9] L. Adamczyk *et al.* (STAR Collaboration), *Phys. Rev. Lett.* 121, 032301 (2018).
- [10] G. Aad *et al.* (ATLAS Collaboration), *Phys. Rev. Lett.* 131, 072301 (2023).
- [11] J. F. Gunion and G. Bertsch, *Phys. Rev. D* 25, 746 (1982).
- [12] I. Vitev, *Phys. Rev. C* 75, 064906 (2007).
- [13] Z. B. Kang, I. Vitev, and H. Xing, *Phys. Rev. C* 92, 054911 (2015).
- [14] M. Lushozi, L. D. McLerran, M. Praszalowicz, and G. M. Yu, *Phys. Rev. C* 102, 034908 (2020).
- [15] B. Abelev *et al.* (ALICE Collaboration), *Phys. Lett. B* 719, 29 (2013).
- [16] S. Chatrchyan *et al.* (CMS Collaboration), *Phys. Lett. B* 718, 795 (2013).
- [17] G. Aad *et al.* (ATLAS Collaboration), *Phys. Rev. Lett.* 110, 182302 (2013).
- [18] A. Adare *et al.* (PHENIX Collaboration), *Phys. Rev. Lett.* 111, 212301 (2013).
- [19] K. Werner, I. Karpenko, and T. Pierog, *Phys. Rev. Lett.* 106, 122004 (2011).
- [20] K. Werner, I. Karpenko, T. Pierog, M. Bleicher, and K. Mikhailov, *Phys. Rev. C* 83, 044915 (2011).
- [21] C. Shen, J. F. Paquet, G. S. Denicol, S. Jeon, and C. Gale, *Phys. Rev. Lett.* 116, 072301 (2016).
- [22] C. Shen, J. F. Paquet, G. S. Denicol, S. Jeon, and C. Gale, *Phys. Rev. C* 95, 014906 (2017).
- [23] S. Sadhu and P. Ghosh, *Phys. Rev. D* 99, 034020 (2019).
- [24] H. Abramowicz and A. C. Caldwell, *Rev. Mod. Phys.* 71, 1275 (1999).
- [25] J. Kapusta, P. Lichard, and D. Seibert, *Phys. Rev. D* 44, 2774 (1991).
- [26] T. Peitzmann, M. H. Thoma, *Phys. Rep.* 364, 175 (2002).
- [27] J. F. Owens, *Rev. Mod. Phys.* 59, 465 (1987).
- [28] A. Adare *et al.* (PHENIX Collaboration), *Phys. Rev. C* 91, 064904 (2015).
- [29] A. Adare *et al.* (PHENIX Collaboration), *Phys. Rev. Lett.* 104, 132301 (2010).
- [30] S. Turbide, C. Gale, S. Jeon, and G. D. Moore, *Phys. Rev. C* 72, 014906 (2005).
- [31] J. Adam, *et al.* (ALICE Collaboration), *Phys. Lett. B* 754, 235 (2016).
- [32] L. Yan, *Phys. Rev. C* 91, 064909 (2015).
- [33] S. Chatrchyan, *et al.* (CMS Collaboration), *Phys. Rev. C* 84, 024906 (2011).
- [34] J. Pumplin, D. R. Stump, J. Huston, H. L. Lai, P. Nadolsky, and W. K. Tung, *JHEP* 07, 012 (2002).
- [35] K. J. Eskola, H. Paukkunen, and C. A. Salgado, *JHEP* 04, 065 (2009).
- [36] E. Braaten and R. D. Pisarski, *Nucl. Phys. B* 337, 569 (1990).
- [37] R. Baler, H. Nakkagawa, A. Niegawa, and K. Redlich, *Z. Phys. C*, 53, 433 (1992).
- [38] J. Alam, D. K. Srivastava, B. Sinha, and D. N. Basu, *Phys. Rev. D* 48, 1117 (1993).
- [39] P. Arnold, G. D. Moore, and L. G. Yaffe, *JHEP* 12, 009 (2001).
- [40] P. Aurenche, F. Gelis, H. Zaraket, and R. Kobes, *Phys. Rev. D* 58, 085003 (1998).
- [41] F. D. Steffen and M. H. Thoma, *Phys. Lett. B* 510, 98 (2001).
- [42] J. K. Nayak and B. Sinha, *Phys. Lett. B* 12, 110 (2013).
- [43] J. F. Paquet, C. Shen, G. S. Denicol, M. Luzum, B. Schenke, S. Jeon, and C. Gale, *Phys. Rev. C* 93, 044906 (2016).
- [44] S. Turbide, R. Rapp, and C. Gale, *Phys. Rev. C* 69, 014903 (2004).
- [45] J. Alam, P. Roy, and S. Sarkar, *Phys. Rev. C* 71, 059802 (2005).
- [46] M. Heffernan, P. Hohler, and R. Rapp, *Phys. Rev. C* 91, 027902 (2015).
- [47] R. J. Fries, B. Müller, and D.K. Srivastava, *Phys. Rev. Lett.* 90, 132301 (2003).
- [48] R. J. Fries, B. Müller, and D.K. Srivastava, *Phys. Rev. C* 72, 041902(R) (2005).
- [49] S. Turbide, C. Gale, D. K. Srivastava, and R.J. Fries, *Phys. Rev. C* 74, 014903 (2006).
- [50] S. Turbide, C. Gale, E. Frodermann, and U. Heinz, *Phys. Rev. C* 77, 024909 (2008).
- [51] Y. P. Fu and Q. Xi, *Phys. Rev. C* 92, 024914 (2015).